Modeling Aeolian Tones by Global Instability Modes

Robin Prinja, Peter Jordan, Florent Margnat

Modeling Aeolian Tones by Global Instability Modes

Robin Prinja*, Peter Jordan † and Florent Margnat ‡
Institut Pprime, Département Fluides, Thermique, Combustion - Université de Poitiers, ISAE-ENSMA, CNRS, Poitiers, 86073, France

A noise prediction approach is proposed for bluff body wakes such as flow over a cylinder, where the primary noise source comprises of large scale coherent structures such as the vortex shedding flow feature. With the aim of developing low-order noise models, the strategy of this work is to extract and model such coherent structures. The modeling is based on a linear global stability analysis on the time-averaged mean flow to extract the dominant structures, whose amplitudes are then calibrated via two-point statistics. Curle's analogy is then implemented for far-field noise predictions. The overall approach is validated for flow over a circular cylinder for two cases of Reynolds numbers, Re =150 **and** 13000**, and the noise predictions are found to be** $<$ 2dB **off from the actual measurements.**

I. Introduction

The aim of this work is to develop low-order noise prediction models for airframe-generated noise, which is a major noise source during the landing phase of the commercial aircrafts. Landing gear and high lift devices such as trailing-edge flaps, leading-edge slats etc. are the primary contributors to the airframe noise [1]. Similar noise sources can be found in various other moving bodies such as a car's rear view mirror and an electric train's pantograph.

We intend to formulate fast-return physics-based reduced-order models that can predict far-field noise from bluff-bodies such as circular cylinders. We seek the models to be accurate and robust so that once developed for the canonical bodies, they can be straightforwardly evolved for complex bodies and be used for low-cost diagnostics at the design step.

The bluff-body noise, from flow over a circular cylinder for instance, is a tonal noise generated by the periodic flow distortions associated with the interaction of wakes, the phenomenon which is popularly known as von Kármán vortex street. This phenomenon shows a stream of alternately rotating vortices that perseveres till many diameters downstream. First studied by Strouhal [2], the frequency of tonal noise from this vortex shedding is given as,

$$f = St \times \frac{U_\infty}{d}, \tag{1}$$

where St is the Strouhal number, U_∞ is the free-stream velocity and d is the cylinder diameter. This vortex shedding based tonal noise feature is inherent in the wake flows ranging from low Reynolds number ($Re = U_\infty d/\nu$, ν is the dynamic viscosity) flows to high-Re turbulent flows [3].

The vortex shedding (VS) can be seen as a global instability in the flow-field [4, 5]. The frequency of vortex shedding and spatial structure of the fluctuations can be deduced by performing linear global instability analysis on the time-averaged mean flow [6–8]. The spatio-temporal structures of vortex shedding fluctuations can then be used to predict the far-field noise by using an acoustic analogy. Acoustic analogies [9–11] simplify the noise prediction problem to an emitter-receiver problem which is much less expensive that the direct numerical methods that contain the whole space as their computational grid.

The paper is organised as follows. Section II presents the proposed noise predictiong methodology which is a multi-step approach. First step is to get the time-averaged mean velocity field. Second step is to perform the linear global stability analysis on this mean flow and the calibration of their mode amplitudes as presented in section II.A. Third step is to use an acoustic analogy to predict far-field noise as presented in section II.B. Section III presents the applications of the noise modeling approach for the two cases i.e. Re = 150 and 13000 flow over a circular cylinder.

*Graduate Student, robin.prinja@univ-poitiers.fr
†Research Director, peter.jordan@univ-poitiers.fr
‡Assistant Professor, florent.margnat@univ-poitiers.fr

II. Modeling approach

Here, we present the methodology to develop the noise prediction models for the wake problems such as flow over a cylinder which leads to tonal far-field noise. The model is based on a multistep hybrid approach that requires very less computational time and memory storage as compared to the high-fidelity methods such as Direct Numerical Simlation (DNS) or Large Eddy Simulation (LES).

A. Modeling the dominant hydrodynamic fluctuations by global stability analysis

The flow fluctuations behind the far-field tonal noise i.e. the vortex shedding structures, are modeled by linear global stability analysis around the mean flow to obtain their spatial structures and fluctuation frequencies. Global stability analysis based on linear analysis is an initial value problem for infinitesimal perturbations [4, 12]. It assumes a known base flow, which could be time-averaged velocity field, $\overline{\mathbf{U}}$ (as in the present work), or steady state solution of the Navier-Stokes equations, that can be provided by a preliminary simulation or an experiment [7].

Global stability analysis seeks for the eigenbasis of the Fourier decomposed fluctuations that the flow field can sustain. Decomposing the flow variables into their mean and fluctuating components and using them in the incompressible Navier Stokes leads to the Incompressible Linear Navier Stokes (LNS) system given as,

$$\begin{aligned} \nabla \cdot \mathbf{u} &= 0, \\ \frac{\partial \mathbf{u}}{\partial t} + (\mathbf{u} \cdot \nabla)\overline{\mathbf{U}} + (\overline{\mathbf{U}} \cdot \nabla)\mathbf{u} &= -\nabla p + \frac{1}{Re}\Delta \mathbf{u}, \end{aligned} \tag{2}$$

where $\overline{\mathbf{U}}$ and $\mathbf{u}$ are the mean and fluctuating parts of the velocity vector respectively, and p is the pressure fluctuation. The system (Eq. 2) can be written in compact form as,

$$\frac{\partial \mathbf{u}}{\partial t} = \mathbf{A}(\overline{\mathbf{U}})\mathbf{u}, \tag{3}$$

where $\mathbf{A}(\overline{\mathbf{U}})$ is the linear operator.

We use the normal mode ansatz for fluctuations as,

$$\mathbf{u}(x, y, z, t) = \hat{\mathbf{u}}(x, y)e^{ikz}e^{-i\lambda t}, \tag{4}$$

where $\hat{\mathbf{u}}$ is the spatial structure of the global mode; λ is the eigenvalue of the system whose real and imaginary parts represent the frequency and growth rate respectively of the global mode; k is the spanwise wavenumber; and x, y and z are the spatial coordinates in streamwise, transverse and spanwise directions respectively.

Using the ansatz in Eq. 3 leads to an eigenvalue problem,

$$\mathbf{A}\hat{\mathbf{u}} = -i\lambda\hat{\mathbf{u}}. \tag{5}$$

For the present work, the eigensystem (Eq. 5) is solved by using Nektar++ package [13] based on Arnoldi's method [14].

As the stability analysis is linear, we need to calibrate subsequently the amplitude of the VS mode. The mode calibration method for a $Re = 13000$ flow is presented in section III.B.3, where the velocity fluctuation field from Time Resolved Particle image velocimetry (TR PIV) is decomposed into its frequency-wavenumber modes and then used to calibrate the global modes.

B. Noise prediction

Noise prediction in our multistep approach employs Curle's analogy [11] which relates the sound to the integral of surface source terms, once volume source terms have been neglected in this low Mach number case. As we have evaluated the noise sources in the previous step, the sound field can be directly computed using the analogy.

3D Curle's analogy in frequency space is given as,

$$\hat{p}(\mathbf{x}_o, f) = -\iint_S \hat{p}(\mathbf{x}_s, f)\left(\frac{\partial G}{\partial \mathbf{x}_s} \cdot \mathbf{n}\right) dS(\mathbf{x}_s), \tag{6}$$

where $\hat{p}(\mathbf{x}_o, f)$ is the noise prediction at the observer location ($\mathbf{x}_o$) in the far-field,
$\hat{p}(\mathbf{x}_s, f)$ is the pressure of the global mode at source i.e. cylinder surface ($\mathbf{x}_s$),
$\mathbf{n}$ is the unit surface normal vector at $\mathbf{x}_s$,
G is the free-field Green function given as, $G(\mathbf{x}_o \mid \mathbf{x}_s, f) = -\frac{e^{-ik_a|\mathbf{x}_o - \mathbf{x}_s|}}{4\pi|\mathbf{x}_o - \mathbf{x}_s|}$,
$k_a = f/c_o$ is the acoustic wavenumber and c_o is the free-stream sound speed.

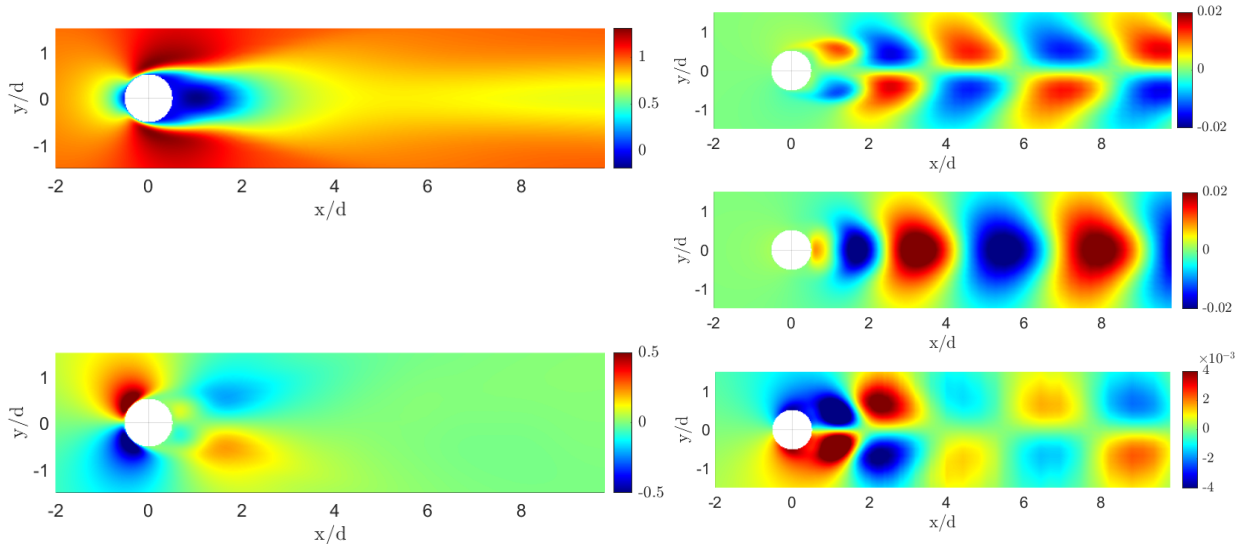

(a) Time-averaged mean flow ($\overline{U}/U_\infty$(top) and $\overline{V}/U_\infty$(bottom)).

(b) Uncalibrated VS global mode structure: Real part of $\hat{u}/U_\infty$ (top), $\hat{v}/U_\infty$ (middle) and $\hat{p}/U_\infty^2$ (bottom).

Fig. 1 $Re = 150$ **flow over a circular cylinder.**

III. Application for circular cylinder flows

In this section, the noise modeling approach has been applied for the case of noise prediction from flow over a circular cylinder. We present the results for time-averaged mean flow, spatial structure and wavenumber of the VS global mode, global mode calibration, and the far-field noise prediction. Before working on $Re = 13000$ flow, the noise modeling approach is first tested for a case of $Re = 150$ flow.

A. $Re = 150$ flow over a circular cylinder

The test case of $Re = 150$ flow over cylinder has been chosen because it has already been widely studied in the past decades. This gives us access to the numerous results in the well-accepted literature against which we can verify the accuracy of our methods. Another reason being that at low Re, the cylinder wakes are much more regular and easier to deduce as compared to the high Re cases where the wakes are irregular and turbulent.

Most of the work for $Re = 150$ has been performed by employing the Nektar++ package [13] that is based on spectral/hp element framework.

1. Mean flow evaluation

The computational domain was kept as $-45 < x/d < 120, -45 < y/d < 45$. The mesh was very refined near the cylinder ($\Delta x/d = 0.017$) and very coarse at the domain boundaries ($\Delta x/d = 1.2$). Inlet uniform velocity was kept at left boundary while all the other boundaries were kept as pressure outlets. Flow was evolved for 200 acoustic time units, via incompressible Navier Stokes solver of the Nektar++ package, to achieve the statistically steady state. The evaluated time-averaged mean flow field, streamwise velocity ($\overline{U}$) and transverse velocity ($\overline{V}$), as shown in Fig. 1a matched well with the findings of Fani et al. [8].

2. Global stability analysis

For $Re = 150$ case, the eigensystem (Eq. 5) was found to be globally stable for the homogeneous spanwise modes i.e. $k = 0$. The spatial structures of the least stable global mode are shown in Fig. 1b, and its eigenvalue was found as, $\lambda \times d/U_\infty = 1.1443 - 0.0004i$ which corresponds to $St = 0.1821$. This value is in agreement with $St = 0.183$ from the compressible DNS by Inoue & Hatakeyama [15] and $St = 0.189$ in the incompressible simulation by Margnat [16]. The eigenstructures were in agreement with Fani et al. [8]. The mode structure and St indicate that this is the one that corresponds to the vortex street period.

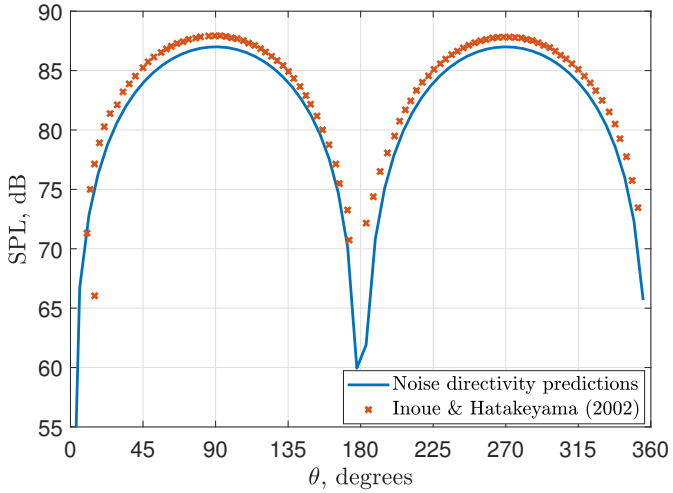

Fig. 2 SPL directivity predictions at $r/d = 75$ for $Re = 150$ flow over a circular cylinder. Streamwise direction corresponds to $\theta = 0$.

3. Mode calibration

For the $Re = 150$ case, various probes were kept in the region $-1 < x/d < 3$, $0.1 < y/d < 1.5$ to record the time-history of p. The global mode amplitude was then calibrated with the pressure fluctuation amplitudes at the probe locations in the direct simulation. The calibration ratio was found to be nearly independent of the location of the calibration point in the considered domain as calibration ratio varied as, $r_{cal} = 36 \pm 8$.

4. Noise prediction

The noise predictions were evaluated at the microphone locations which are distributed along a circular arc of radius $r/d = 75$ centered at cylinder center. 3D Curle's analogy was used, as presented in the Eq. 6, where the 2D global mode pressure fluctuations were homogeneously distributed along the cylinder's spanwise length of ± 10000 diameters.

The results are shown in Fig. 2 for Sound Pressure Level (SPL) from the global mode with a calibration ratio, $r_{cal} = 36$. The pressure directivity clearly shows its dipole nature as expected from Curle's approach for such a low drag geometry. Figure 2 also shows comparison with the output of a compressible DNS for $Re = 150$, Mach number, $M = 0.2$ [15]. The close agreement of our model with the direct noise computation encourages us to apply it to a higher Re case.

B. $Re = 13000$ flow over a circular cylinder

Flow over a circular cylinder ($d = 0.01$m) at $Re = 13000$ is studied here which consists of turbulent wake and tonal noise characteristics. Flow configuration can be seen in Fig. 3. The flow consists of $U_\infty = 20$m/s airflow at NTP conditions exiting from the nozzle section 70×70cm with turbulent intensity of 0.5% at 30cm downstream, where the cylinder is mounted. The origin of coordinate system is kept at the cylinder center. The wind-tunnel jet is along $x-$axis and cylinder's span is along $z-$axis.

To measure the time-averaged mean velocity field, a Particle image velocimetry (PIV) system has been setup in the mid-span XY plane (domain shown in blue in Fig. 3 (left)). To study the fluctuation velocity field, a TR-PIV system is setup in the XZ plane at $y/d = 1$ (domain shown in green in the Fig. 3 (right)). A microphone is kept at $x/d = 0, y/d = 100, z/d = 0$ to record the far-field acoustics.

1. Mean flow evaluation

The first step of our noise modeling approach is to obtain the time-averaged mean flow in the XY plane. This can be achieved via PIV experiments or via Reynolds-averaged Navier–Stokes (RANS) equations based solvers such as STAR-CCM+. For the present work, this has been achieved by PIV system setup in the mid-span XY plane as shown in the Fig. 3(left). The experiments setup consists of: (i) High resolution camera *Phantom VEO 4K 990L* (4096×2304

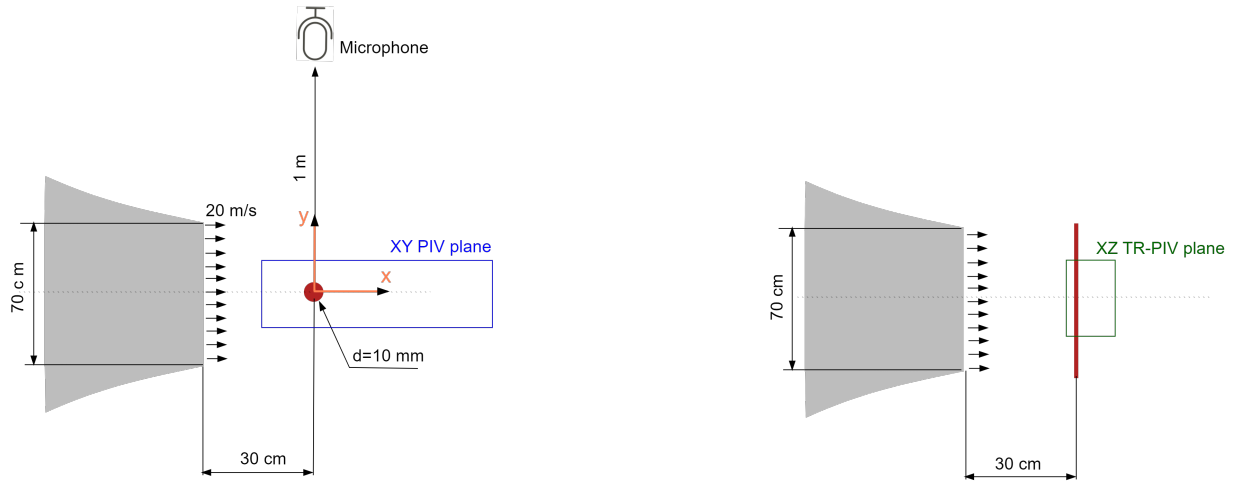

Fig. 3 Schematic diagram for $Re = 13000$ flow over a circular cylinder (not to scale). Front view (at left) and top view (at right) are shown.

pixels), and the images were taken with a sampling frequency of 100Hz . (ii) Laser Continuum Terra PIV (2 x 30 mJ), synchronised with the camera, was used to illuminate periodically the seeding; the time-delay between two consecutive laser illuminations was kept as 10μs so as to capture the important fast scale motions.

For data analysis, LaVision Davis 10 software was used to get the velocity field and the steady-state statistics. The interrogation window size was kept as 32×32 pixels and 75% overlap. This yielded the PIV domain of $[-11 < x/d < 11$, $-2 < y/d < 2$] with spatial resolution of $\Delta x/d = \Delta y/d = 0.0235$; and 6000 time-steps were recorded, leading to acquisition time of 60s to ensure the convergence of mean statistics.

Before moving to the next step, the mean flow was post-processed in following ways: (i) due to the high reflection at the cylinder's surface, the flow velocities very close to the cylinder's surface were unavailable, so the boundary condition (zero velocity) was forced there; (ii) the data smoothing was done based on the Helmholtz smoothing projection method (using a Nektar++ code package [13]) so as to avoid the non-physical highly unstable global modes during the instability calculations in the next step.

The final mean flow is shown in Fig. 4a where streamwise and transverse velocities are shown. In comparison to the $Re = 150$ mean flow (Fig. 1a), the recirculation region and downstream wake here are much less stretched in x as well as y directions.

The centerline mean streamwise velocity profile is compared against the present literature [17, 18] in Fig. 5. We found a close match with the LES [18] that was performed at almost the same Reynolds no. The experimental data from LDV [17] does not seem to have a good match which could be due to difference in Re (mean flow profiles are highly sensitive to the Re).

2. Global stability analysis

For the case of $Re = 13000$ also, the eigensystem (Eq. 5) was found to be globally stable for the homogeneous spanwise stability analysis, $k = 0$. The spatial structures of the least stable global mode, which corresponds to the vortex-shedding mode, are shown in Fig. 4b. The structures clearly shows the vortex shedding feature. As compared to the $Re = 150$ global mode, the structures are more and more pulled in the downstream direction as we move closer to the $y = 0$ axis. The eigenvalue for this mode, $\lambda = 1.3575 - 0.1251i$ which corresponds to $St = 0.216$, is close to the dominant fluctuation frequency in the flow field and also to the tonal far-field noise frequency (Pinto et al. [19]).

3. Mode calibration

To obtain the amplitudes for the global modes, the fluctuation field in the XZ plane has been used to extract the large-scale dominant coherent structures. Here, the high speed TR PIV setup in the XZ plane at $y/d = 1$ (as shown in the Fig. 3) is employed to characterize the flow dynamics. The experiments setup consists of: (i) Two high speed

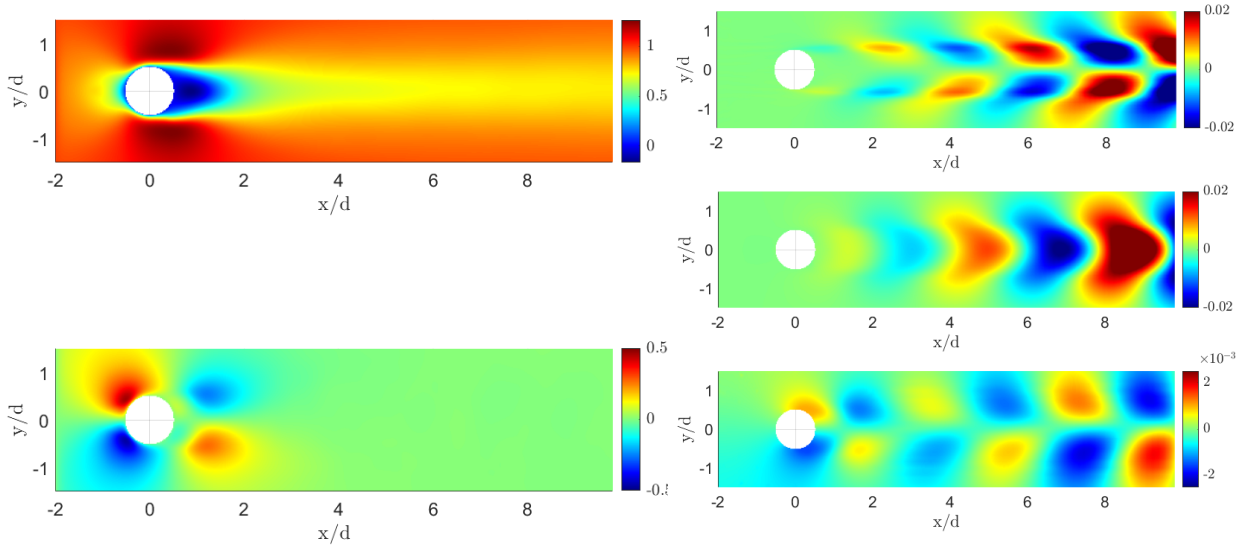

(a) Time-averaged mean flow ($\overline{U}/U_\infty$(top) and $\overline{V}/U_\infty$(bottom)).

(b) Uncalibrated VS global mode structure: Real part of $\hat{u}/U_\infty$ (top), $\hat{v}/U_\infty$ (middle) and $\hat{p}/U_\infty^2$ (bottom).

Fig. 4 $Re = 13000$ **flow over a circular cylinder.**

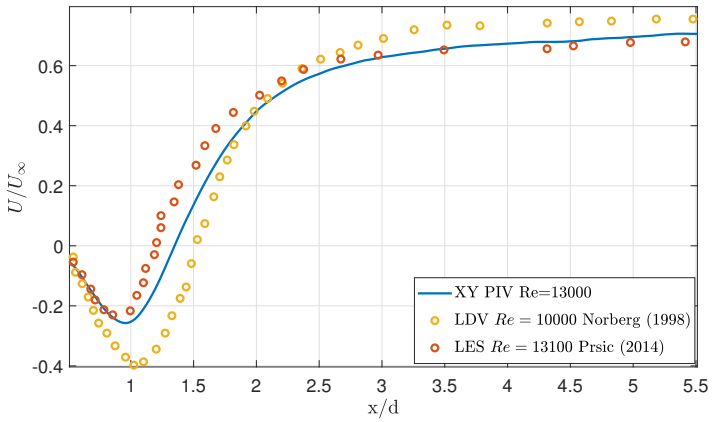

Fig. 5 $Re = 13000$ **XY PIV: mean streamwise velocity profile,** $\overline{U}/U_\infty$**, at** $y/d = 0$**.**

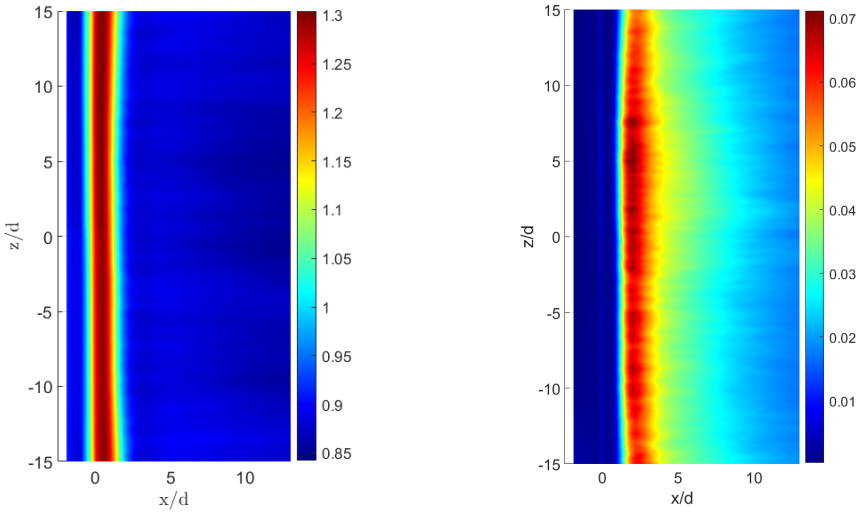

(a) Mean streamwise velocity, $\overline{U}/U_\infty$. **(b) Mean reynolds stress, R_{xx}/U_∞^2.**

Fig. 6 $Re = 13000$ **XZ TR-PIV at** $y/d = 1$**: mean flow statistics.**

cameras *Photron Fastcam SA-Z* (1024×1024 pixels) placed side by side taking images at the sampling frequency of 20kHz . (ii) Continuum Mesa PIV (2 x 9 mJ) laser, synchronised with the camera; the time-delay between two consecutive laser illuminations was kept as 20μs.

Velocity fields from PIV images were obtained from LaVision Davis 10 software with the interrogation windows size of 16×16 pixels and 75% overlap. Finally, we have 22000 time-steps of velocity field with sampling frequency of $F_s = 10$kHz in the spatial domain $[-2 < x/d < 14, -15 < z/d < 15\,]$, with spatial resolution of $\Delta x/d = \Delta z/d = 0.1263$. The spanwise homogeneity and convergence of the turbulent statistics were assured.

Subtracting its mean component from the velocity time-series data, we obtain the fluctuation time-series ($\mathbf{u} = \mathbf{U} - \overline{\mathbf{U}}$). The fluctuation time-series was then split into 215 realizations, where each realization contains 400 snapshots and overlap of 75%. It was then decomposed into Fourier modes in the frequency domain using Eq. 7. This leads to frequency resolution of $\Delta St = \Delta f d/U_\infty = 0.0125$.

$$\mathbf{u}(x, z, t) = \sum_{\omega} \hat{\mathbf{u}}_\omega(x, z)\ e^{i\omega t}, \tag{7}$$

where ω is the angular frequency of the fourier modes. Figure 6 shows mean flow stastistics for streamwise velocity, $\overline{U}$ and reynolds stress, $R_{xx} = \rho\overline{u^2}$.

An instantaneous snapshot for the streamwise velocity fluctuation is shown in Fig. 7a. Large scale coherent structures can be clearly observed hinting the system to be of low order. For the mid-span axis, $z/d = 0$, the power spectral density (PSD) colormap for streamwise-velocity fluctuations is shown in Fig. 7b. Figure 7b shows that a single frequency, $St \approx 0.2$, that corresponds to the VS period, is dominating the fluctuation field and this was found to be same for all the spanwise locations.

The cross spectral density (CSD) of the streamwise velocity fluctuation field, is then calculated as,

$$S_{z_0 z, \omega}(x) = \hat{u}_\omega(x, z_0)\, \hat{u}^*_\omega(x, z), \tag{8}$$

where $z_0 = 0$ is chosen as the reference position and * represents the complex conjugate. The magnitude of CSD for $St = 0.2$ is shown in Fig. 7c.

The CSD is then decomposed into its spanwise Fourier modes as,

$$S_{z_0 z, \omega}(x) = \sum_{k=-\infty}^{\infty} \tilde{S}_{k,\omega}(x)\ e^{ikz}, \tag{9}$$

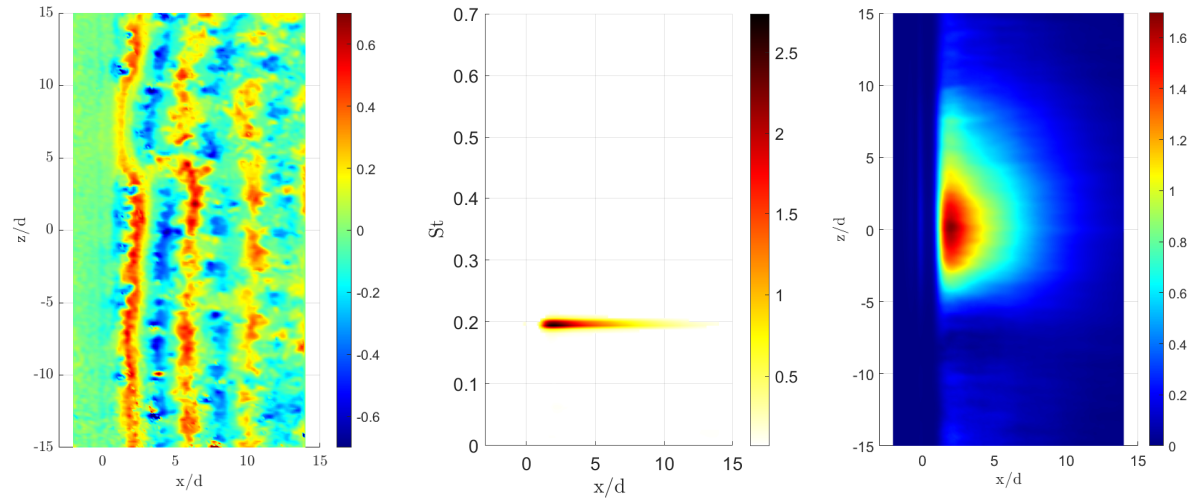

(a) u/U_∞**, at a time-instant.** **(b)** $\hat{u}\hat{u}/{U_\infty}^2$ **PSD at** $z/d = 0$**.** **(c)** $S_{z_0 z}/U_\infty^2$ **for** $St = 0.2, z_0 = 0$**.**

Fig. 7 $Re = 13000$ **XZ TR PIV at** $y/d = 1$**: streamwise velocity fluctuations** (u)**.**

where $\tilde{S}_{k,\omega}$ can be evaluated from CSD as,

$$\tilde{S}_{k,\omega}(x) = \frac{1}{L} \sum_{z=-L/2}^{L/2} S_{z_0 z,\omega}(x)\ e^{-ikz}\ \Delta z, \tag{10}$$

where $L = 70d$ is the cylinder's spanwise length (defined as the periodic length of the system) and Δz is the spanwise resolution. The bandlimited power spectrum (BPS), for $St = 0.2 \pm 2.5\%$, is shown in Fig. 8 which peaks near $x/d \approx 2$ which is same as the peak R_{xx} location. Also, it shows the low-rank behaviour i.e. only $\mid k \mid \leq 5$ spanwise wavenumbers are important. Then the linear global instability mode is calibrated by multiplying with a calibration ratio, r_{cal}, such that the global mode power is same as the $\tilde{S}$ BPS . For $k = 0$ global instability mode, the calibration ratio in the region $0.5 < x/d < 3$ is $r_{cal} = 41 \pm 18$, as shown in Fig. 9.

4. Noise prediction

Final step of the modeling approach is to predict noise in the far-field following the procedure presented in the section II.B. At $r/d = 100$, noise directivity SPL predictions are shown in the Fig. 10, where the global mode calibration ratio was taken as $r_{cal} = 41$.

The noise measurements at $x/d = 0, y/d = \pm 100$ are also shown (with crosses), which were recorded with a microphone with a sampling frequency of 50kHz and acquisition time of $6s$ during the wind-tunnel experiments (Fig. 3). The measured noise SPL was calculated from the BPS in the range, $St = 0.2 \pm 25\%$, where the dominant tone was located. Also, acoustic measurements by Pinto [20], for the same flow configuation and BPS for the same St range, are shown (with circles). Fig. 10 shows that the noise measurements are less than 1dB off from the measurements.

IV. Conclusion

A linear global stability analysis based noise modeling was presented in order to predict bluff-body noise where the interaction of flow with a cylindrical body leads to tonal noise. Modelling approach was applied for a canonical problem of flow over a circular cylinder for two cases of flow-velocities, $Re = 150$ and $Re = 13000$. The global modes from the stability analysis on mean flow for both the cases were evaluated. The modes were found to be characterising the vortex-shedding feature of the flow-field, that corresponds to the dominating fluctuations and tonal noise. For $Re = 150$ flow, the global mode was then calibrated and noise prediction was found to be in accordance with the present literature.

For $Re = 13000$ flow, the calibration and noise prediction results were also presented. For this case, the frequency-wavenumber decomposition of the fluctuation field from the TR-PIV in the XZ plane was found be a low rank system

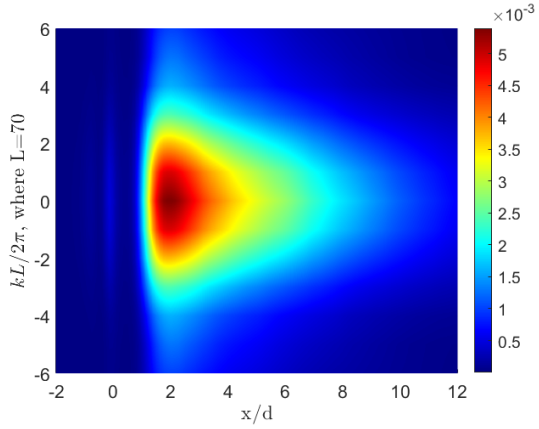

Fig. 8 $Re = 13000$ **XZ TR PIV at** $y/d = 1$**:** $\tilde{S}/U_\infty^2$ **BPS for** $St = 0.2 \pm 2.5\%$**.**

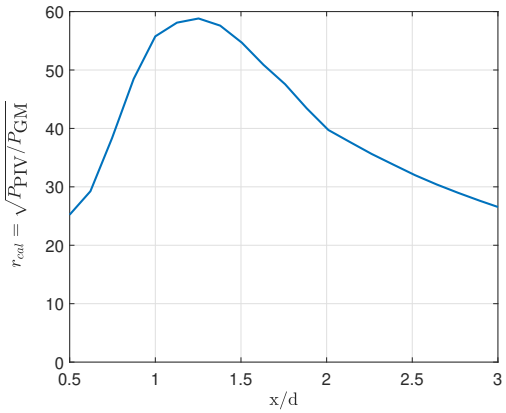

Fig. 9 $Re = 13000$ **VS global mode calibration ratio.** $P_{\mathbf{PIV}} = \widetilde{S}/U_\infty^2$ **BPS;** $P_{\mathbf{GM}} = \frac{1}{2} \mid \hat{u} \mid^2 / U_\infty^2$**.**

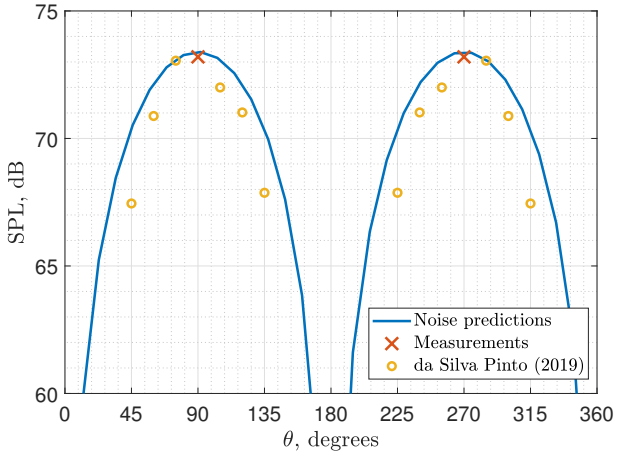

Fig. 10 $Re = 13000$ **SPL directivity predictions at** $r/d = 100$**. Streamwise direction corresponds to** $\theta = 0$**.**

which hints that, with very few global instability modes, we can accurately represent the fluctuation field and predict the far-field noise. Far-field noise directivity predictions with homogeneous spanwise mode were made which were found to be very close to the noise measurements. The issue of uncertainty in the mode calibration ratio, that arises from its dependence on the spatial location, needs to be investigated further.

References

[1] Li, Y., Wang, X., and Zhang, D., "Control strategies for aircraft airframe noise reduction," *Chinese Journal of Aeronautics*, Vol. 26, No. 2, 2013, pp. 249–260.

[2] Strouhal, V., *Über eine besondere Art der Tonerregung*, Stahel, 1878.

[3] Williamson, C. H., "Vortex dynamics in the cylinder wake," *Annual review of fluid mechanics*, Vol. 28, No. 1, 1996, pp. 477–539.

[4] Huerre, P., and Monkewitz, P. A., "Local and global instabilities in spatially developing flows," *Annual review of fluid mechanics*, Vol. 22, No. 1, 1990, pp. 473–537.

[5] Chomaz, J.-M., "Global instabilities in spatially developing flows: non-normality and nonlinearity," *Annu. Rev. Fluid Mech.*, Vol. 37, 2005, pp. 357–392.

[6] Giannetti, F., and Luchini, P., "Structural sensitivity of the first instability of the cylinder wake," *Journal of Fluid Mechanics*, Vol. 581, 2007, pp. 167–197.

[7] Sipp, D., and Lebedev, A., "Global stability of base and mean flows: a general approach and its applications to cylinder and open cavity flows," *Journal of Fluid Mechanics*, Vol. 593, 2007, pp. 333–358.

[8] Fani, A., Citro, V., Giannetti, F., and Auteri, F., "Computation of the bluff-body sound generation by a self-consistent mean flow formulation," *Physics of Fluids*, Vol. 30, No. 3, 2018, p. 036102.

[9] Lighthill, M. J., "On sound generated aerodynamically I. General theory," *Proceedings of the Royal Society of London. Series A. Mathematical and Physical Sciences*, Vol. 211, No. 1107, 1952, pp. 564–587.

[10] Lighthill, M. J., "On sound generated aerodynamically II. Turbulence as a source of sound," *Proceedings of the Royal Society of London. Series A. Mathematical and Physical Sciences*, Vol. 222, No. 1148, 1954, pp. 1–32.

[11] Curle, N., "The influence of solid boundaries upon aerodynamic sound," *Proceedings of the Royal Society of London. Series A. Mathematical and Physical Sciences*, Vol. 231, No. 1187, 1955, pp. 505–514.

[12] Theofilis, V., "Global linear instability," *Annual Review of Fluid Mechanics*, Vol. 43, 2011, pp. 319–352.

[13] Cantwell, C. D., Moxey, D., Comerford, A., Bolis, A., Rocco, G., Mengaldo, G., De Grazia, D., Yakovlev, S., Lombard, J.-E., Ekelschot, D., et al., "Nektar++: An open-source spectral/hp element framework," *Computer physics communications*, Vol. 192, 2015, pp. 205–219.

[14] Arnoldi, W. E., "The principle of minimized iterations in the solution of the matrix eigenvalue problem," *Quarterly of applied mathematics*, Vol. 9, No. 1, 1951, pp. 17–29.

[15] Inoue, O., and Hatakeyama, N., "Sound generation by a two-dimensional circular cylinder in a uniform flow," *Journal of Fluid Mechanics*, Vol. 471, 2002, pp. 285–314.

[16] Margnat, F., "Hybrid prediction of the aerodynamic noise radiated by a rectangular cylinder at incidence," *Computers & Fluids*, Vol. 109, 2015, pp. 13–26.

[17] Norberg, C., "LDV-measurements in the near wake of a circular cylinder," *ASME Paper No. FEDSM98-521*, 1998, pp. 41–5.

[18] Prsic, M. A., Ong, M. C., Pettersen, B., and Myrhaug, D., "Large Eddy Simulations of flow around a smooth circular cylinder in a uniform current in the subcritical flow regime," *Ocean Engineering*, Vol. 77, 2014, pp. 61–73.

[19] Pinto, W. J., Margnat, F., and Gervais, Y., "Effect of cross-section on flow three-dimensionality for prismatic bodies and the associated noise emission," *25th AIAA/CEAS Aeroacoustics Conference*, 2019, p. 2531.

[20] da Silva Pinto, W. J. G., "Modelling airframe noise: from aerodynamic topology to acoustic efficiency," Ph.D. thesis, Université de Poitiers, 2019.